A 4-DoF parallel robot with a built-in gripper for waste sorting

Maxence Leveziel[1], Guillaume J. Laurent[1], Wissem Haouas[1], Michael Gauthier[1] and Redwan Dahmouche[1]

Abstract—This article presents a new robot concept dedicated to fast and energy-efficient waste sorting applications. This parallel robot can provide at the same time the three translations in space (3-DoF) and the opening/closing of a built-in gripper (1 additional DoF). The movement of the clamp is enabled thanks to a configurable platform at the end of the parallel structure. This platform is composed of a two-gear train gripper which is directly controlled by the 4 actuators attached to the base of the manipulator. The inverse kinematic as well as the differential models have been developed. A first prototype has been realized to validate this new parallel architecture for pick-and-toss tasks.

Keywords—*Mechanism Design; Parallel Robots; Industrial Robots*

I. Introduction

RECYCLING and recovery of waste is a major environmental issue to reduce the human impact on the environment. Recently, robotized waste sorting machines have begun to replace human operators in material recovery facilities (MRFs) and other recycling centers [1], [2]. These machines rely on computer vision for the identification of a class of waste from RGB and hyperspectral camera images. The advances in deep learning enable the identification and separation with an efficiency of up to 95% of the targeted material on the conveyor belt [3]. Then, fast pick-and-toss robots are used to capture the waste directly from the material stream.

The main advantage is the reduction of manpower issues such as the dependency on manual sorters within a facility and the protection of workers from exposure to high-risk handling situations (injury, contamination, musculoskeletal disorder). Other benefits are the improvement of sorting quality, continuous sorting, the increase of recovery rates, and the minimization of pre-shredding.

A few companies offer automated sorting machines for MRFs. AMP Robotics, Bulk Handling Systems (BHS), Machinex, TOMRA Sorting Recycling, and ZenRobotics are among those focusing on computer vision and robotics. They all make use of standard industrial robots for picking

Figure 1. Example of parallel robots in action in the waste sorting machine from AMP robotics (Ix4 Omron robot equipped with the P30 rigid platform) [8].

objects. Currently, these sorting machines can reach pick rates almost double that of a human operator (respectively 70 ppm vs. 30 to 40 ppm) [4]. To reduce the costs and the energy consumption of the sorting, the robots must be fast and more energy efficient.

Parallel mechanisms have been adopted to meet these needs. Thanks to the actuators located on the robot's base, the dynamics of these structures are particularly high with a reduced energy consumption compared to serial robots [5]. In particular, Delta robots are among the fastest, cheapest and lightest robots for pick and place operations [6], [7]. They are also easy to repair and dustproof.

The usual configuration for waste sorting is a Delta robot from ABB or Omron equipped with a suction cup. Such a solution is suitable for picking lightweight and flat wastes (cf. Fig. 1). However, suction systems are far from being energy efficient. In addition, grippers are preferred to suction cups to sort heavy wastes and objects having complex geometries or uneven surfaces. For example, heavy pickers from ZenRobotics can sort construction and demolition wastes, commercial, and industrial wastes with a 3-DoF gantry robot equipped with a large gripper [9]. In general, the grippers are mounted onto Cartesian or articulated robots leading to higher power needs, lower speed, and lower pick rates, typically 30 ppm [10], but also shorter lifetime due to the dusty environment [8].

This paper proposes to address this problem with a fast and energy-efficient new parallel robot dedicated to waste sorting. This parallel kinematics can provide at the

same time the three translations in space (3-DoF) and the opening/closing of a built-in gripper (1 additional DoF). Thus, this manipulator can pick different types of objects without any additional gripper mounted on its platform. In addition to reducing the mass, it removes the need to provide the end-effector with compressed air or electric power. The robot is composed of four revolute actuators linked to an original configurable platform that allows exploiting a local DoF for opening and closing a built-in gripper.

The next section presents the related work on parallel robots with configurable platforms dedicated to gripping. Section III introduces the design of the proposed robot while section IV develops its inverse and differential models. Finally, a proof-of-principle prototype of the manipulator is presented in Section V.

II. Related work

In a waste sorting machine, the robot task consists in picking up objects from the conveyor belt and throwing them in a collecting tray. To do this "pick-and-toss" cycle, three translations are required but rotations are usually not needed since it is not required to place the collected item in a precise location as in a regular pick-and-place cycle [11]. Moreover, if the robot is equipped with a gripper with large claws or with a clamshell bucket, it will be able to pick up objects of all shapes and materials regardless of their orientation. Finally, high speed and low power consumption are expected to reduce the costs of sorting. For this reason, parallel structures such as Delta robots are preferred. Several solutions can be considered to provide the grasping in addition to the 3-DoF of a Delta robot without carrying an additional gripper. Among them, the most attractive ones are to use a configurable platform at the top of the parallel kinematic because it can bring additional DoF to the end-effector with very little extra weight.

The first parallel robots with a configurable platform have been introduced by Pierrot [12], [13] and commercialised by Omron/Adept (under the names Quattro and Ix4). This robot, dedicated to pick-and-place operations, provides 3-DoF in translation and 1-DoF in rotation around Z using 4 axes mounted on the robot's base (Schonflies motion). The rotation is obtained by a configurable parallelogram that replaces the rigid platform of Delta robots. The advantages are weight savings and a good equilibrium between the four identical motors that actuate the robot. Several four limbs parallel robots with a configurable platform, close to the Quattro robot kinematic architecture, have since been proposed to generate Schonflies motions [14]–[17].

Some parallel robots with parallelogram-based platforms have been proposed to actuate a gripper. Yi *et al.* [18] and Hamaza *et al.* [19] investigated a (3+1)-DoF structure with a configurable parallelogram which enables to move two end-effector points in the plane. Lambert *et al.* proposed several haptic devices based on a parallel structure with

configurable platforms. For instance in [20], the parallel kinematics can be moved in the 6-DoF of the space while the configuration of a parallelogram provides a translation between the finger tips, leading to (6+1)-DoF. In the same way, the redundant parallel mechanism of Wen *et al.* [21] allows actuating a gripper in the 6-Dof of the space with large rotational ranges.

Nevertheless, the use of parallelogram-based platforms is not suitable for the operation of large claws. Another type of configurable platforms have been proposed by Gosselin *et al.* consisting of two parts separated by a passive revolute joint [22], [23]. This mobility can be used to get unlimited rotational capabilities of the end-effector or to operate an angular gripper. Our team presented also several parallel kinematics with a foldable platform to remotely operate an angular gripper. In [24], the kinematics generates the 6-DoF in motions and one internal mobility provided by the folding of the platform that can be used for grasping or cutting. [25] presents a (3+1)-DoF spherical parallel wrist that provides three rotations and grasping. By replacing the revolute joint built in the platform by an universal one, it is possible to control 2-DoF grippers in addition the 6-DoF in space leading to (6+2)-DoF [26], [27]. The 2-DoF of the gripper are thus the closing and twisting of the finger tips. None of these kinematics are appropriate to the pick-and-toss of waste because they do not generate the necessary and sufficient combination of DoF, which are three translations plus the opening and closing of a gripper.

In this paper, we propose a new architecture dedicated to waste sorting and that provides three translations and angular grasping through the combined action of four active revolute joints at its base.

III. Design of the robotic structure

The concept was inspired by grippers with geared claws and built in a Delta-like structure. Geared grippers use two toothed wheels rotating in opposite directions with a 1:1 ratio. This ratio gives the opportunity to symmetrically control the opening and the closing of the right and left parts of the gripper. Due to the gear train with this specific ratio, the angles of the left part of the platform and of the right part are always the same. A specific design of the platform integrates this gripper without breaking the stress balance in the whole structure.

Specifically, the manipulator kinematics (see Fig. 2) relies on two levels, the parallel structure, and the configurable platform. The first level is made of four independent arms actuated by revolute actuators and attached to the configurable platform. The configurable platform closes the kinematic chains with two revolute joints and a two-gear train. The axes of rotation of the gears are coincident with those of the revolute joints of the platform. Each arm is a R-2(S-S) chain, that can be replaced by R-2(U-S) or R-U-U, where R stands for a revolute joint, S for a spherical joint and U for a universal joint [28].

The configurable platform consists of three parts: a central part M; a left L; and a right R part (see in Fig.
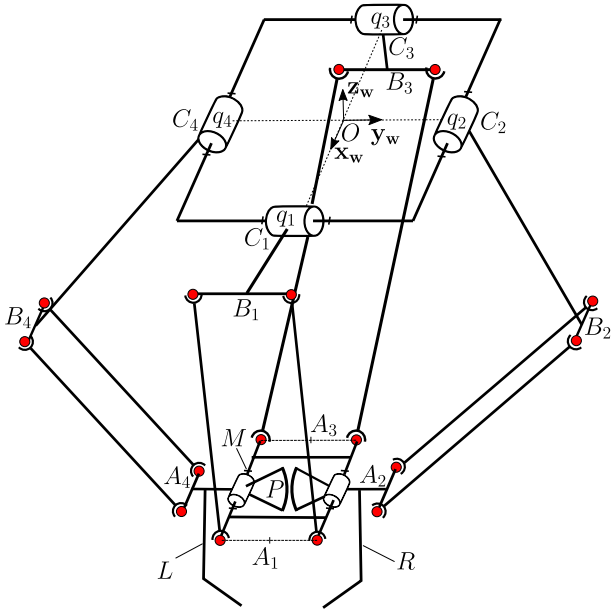
Figure 2. Kinematics design of the 4-DoF manipulator. It is composed of a parallel structure and a configurable platform with a built-in two-gears train gripper. The centers of rotation of the gears are coincident with those of the revolute joints of the platform.
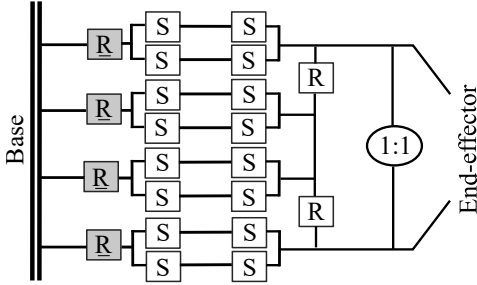

Figure 3. Architectural scheme of the 4-DoF manipulator. $\underline{R}$ stands for an actuated revolute joint, R stands for a passive revolute joint and S stands for a passive spherical joint. 1:1 indicates the gear train ratio between left and right parts of the gripper.

2). The central part M is linked to two kinematic chains and both left L and right R parts by revolute joints. The left L and the right R parts are both linked to a forearm on one side and the center part M on the other side with a revolute joint. The left L and the right R parts hold the gripper claws and rotate symmetrically due to the gear train between them.

The kinematics of the manipulator is illustrated by the architectural scheme in Fig. 3. By construction, the center part of the proposed manipulator cannot rotate in any direction but can translate in the Cartesian frame within the manipulator workspace leading to 3-DoF in displacement. The additional DoF is the symmetrical rotation of the left and right parts of the platform.

IV. Inverse kinematic model and differential model of the manipulator

This section aims to present the inverse kinematic model of the robotic structure and its differential model. The proposed robotic structure ensures that the center part remains horizontal for any configuration of the robot which allows to model each parallelogram with two points spaced with a constant length.

A. Definition of parameters

To model the robotic architecture, several parameters are introduced. The side view of the manipulator and the top view of the platform (see Fig. 4) give a schematic representation of the following parameters:

- q_i is the angle value of the i_{th} rotational actuator. $\mathbf{q}$ stands for the actuators' angles vector;
- k is the distance of the center of rotation of the actuator regarding the origin of the world frame O;
- r is the arms lengths between each C_i and B_i points;
- l is the length of the forearms which corresponds to the distance between B_i and A_i;
- θ is the relative angle between the two parts of the platform;
- u is the half-width of the platform corresponding to the distance between P and A_1 and between P and A_3;
- v is the distance between the center of the platform and the rotation axis of the revolute joints on the platform;
- w is the distance between the axis of rotation of the revolute joint and A_2 (and by symmetry A_4);
- $\mathbf{x} = (x_p; y_p; z_p; \theta)$ is the pose of the manipulator composed of the coordinates of the point P of the platform in the base frame and the angle θ of the configurable platform.
- c_i and s_i stand respectively for $\cos(q_i)$ and $\sin(q_i)$

B. Closure equations

The first part of the modeling is to define the position of all the points of interest in the world frame $\mathcal{W}$ using the parameters previously introduced:

$$\mathcal{W}_{A_1} = \begin{pmatrix} x_p + u \\ y_p \\ z_p \end{pmatrix}; \mathcal{W}_{A_2} = \begin{pmatrix} x_p \\ y_p + v + wc_\theta \\ z_p + ws_\theta \end{pmatrix},$$

$$\mathcal{W}_{A_3} = \begin{pmatrix} x_p - u \\ y_p \\ z_p \end{pmatrix}; \mathcal{W}_{A_4} = \begin{pmatrix} x_p \\ y_p - v - wc_\theta \\ z_p + ws_\theta \end{pmatrix},$$

$$\mathcal{W}_{B_1} = \begin{pmatrix} rc_1 + k \\ 0 \\ rs_1 \end{pmatrix}; \mathcal{W}_{B_2} = \begin{pmatrix} 0 \\ rc_2 + k \\ rs_2 \end{pmatrix},$$

$$\mathcal{W}_{B_3} = \begin{pmatrix} rc_3 - k \\ 0 \\ rs_3 \end{pmatrix}, \mathcal{W}_{B_4} = \begin{pmatrix} 0 \\ rc_4 - k \\ rs_4 \end{pmatrix}.$$

(a) Side view of the manipulator
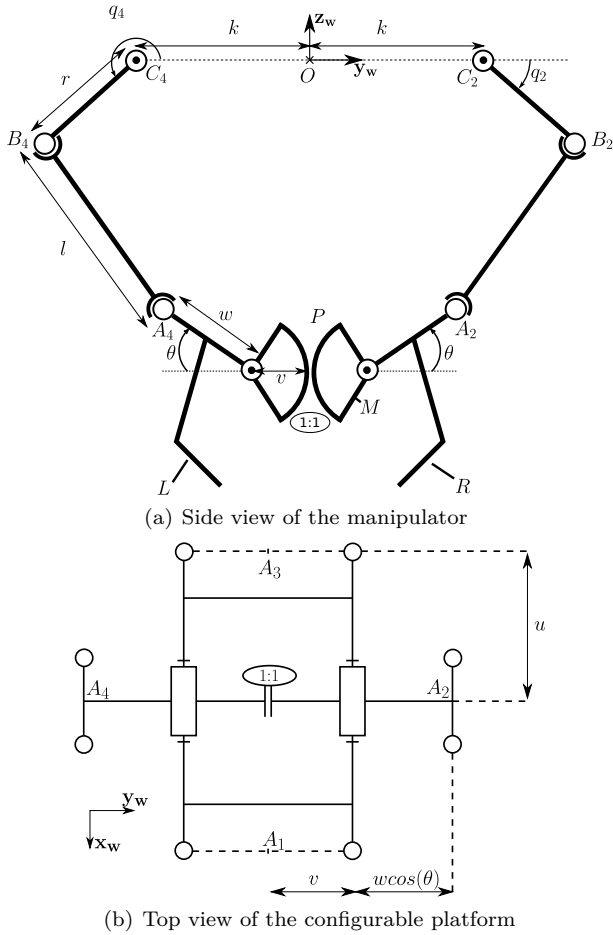

(b) Top view of the configurable platform

Figure 4. Geometry of the manipulator with the localisation of points of interest, design lengths, and the angle between the gripper parts.

With those points corresponding to the extremity of the limbs representing each parallelogram, the closure equations can be written as: $\left\| \overrightarrow{^{\mathcal{W}}A_i\,^{\mathcal{W}}B_i} \right\|^2 = l^2$ with $i \in [1,4]$. For simplicity sake, new variables $(a, b, c, d, e, f, g$ and $h)$ are introduced in the following equations:

$$(\overbrace{x_p+u-k-r\,c_1}^{a})^2 + y_p{}^2 + (\overbrace{z_p-r\,s_1}^{b})^2 = l^2 \qquad (1)$$

$$(\overbrace{x_p-u+k-r\,c_3}^{c})^2 + y_p{}^2 + (\overbrace{z_p-r\,s_3}^{d})^2 = l^2 \qquad (2)$$

$$x_p{}^2 + (\overbrace{y_p+v+w\,c_\theta-k-r\,c_2}^{e})^2 + (\overbrace{z_p+w\,s_\theta-r\,s_2}^{f})^2 = l^2 \qquad (3)$$

$$x_p{}^2 + (\overbrace{y_p-v-w\,c_\theta+k-r\,c_4}^{g})^2 + (\overbrace{z_p+w\,s_\theta-r\,s_4}^{h})^2 = l^2 \qquad (4)$$

Due to the symmetry in the robotic structure, closure equations (1) and (2) are similar as well as (3) and (4). Equations (1) and (2), linking q_1 and q_3 with x_p, y_p and z_p, are typical of a Delta-like robot. But, equations (3) and (4) introduce an additional coupling between q_2 and

q_4 and θ that is not taken into account by usual Delta inverse kinematics.

C. Inverse Kinematic Model

The inverse kinematic model is developed independently for each arm. Each closure equation (equations (1) to (4)) has to be rewritten in the following form [29]:

$$\forall i \in [1,4] \quad D_i\,s_i + E_i\,c_i = F_i. \qquad (5)$$

To obtain these equations, each corresponding closure equation has to be expanded. The expansion yields terms that are factors of either the sine or the cosine or neither. After that, the factors of the sine are collected in D_i, those of the cosine in E_i and the others in F_i.

The equation (5) has several solutions depending on the values of D_i, E_i, and F_i. For the proposed robotic structure, D_i, E_i, and F_i are not zero and the solution is given by:

$$\forall i \in [1,4] \quad \begin{cases} s_i &= \frac{D_i\,F_i+\epsilon\,E_i\sqrt{D_i{}^2+E_i{}^2-F_i{}^2}}{D_i{}^2+E_i{}^2} \\[2mm] c_i &= \frac{E_i\,F_i-\epsilon\,D_i\sqrt{D_i{}^2+E_i{}^2-F_i{}^2}}{D_i{}^2+E_i{}^2} \end{cases} \qquad (6)$$

with $\epsilon = \pm 1$ represents the two solutions for each arm for a given position of the platform. It means that the robot can reach a pose $\mathbf{x} = (x_p; y_p; z_p; \theta)$ if: $\forall i \in [1,4]$,

$$(D_i{}^2 + E_i{}^2 \ge F_i{}^2) \text{ AND } (|s_i| \le 1) \text{ AND } (|c_i| \le 1) \qquad (7)$$

D. Differential model

From the closure equations, the differential model can be derived. Calculating the time derivative of those equations allows to obtain two matrices $\mathbf{J_x}$ and $\mathbf{J_q}$:

$$\mathbf{J_x}\,\dot{\mathbf{x}} = \mathbf{J_q}\dot{\mathbf{q}} \qquad (8)$$

where $\mathbf{J_x}$ and $\mathbf{J_q}$ are respectively the matrices with the coefficient of the time derivative in Cartesian space and in joint space:

$$\mathbf{J_x} = \begin{pmatrix} a & y_p & b & 0 \\ x_p & e & f & f\,w\,c_\theta - e\,w\,s_\theta \\ c & y_p & d & 0 \\ x_p & g & h & h\,w\,c_\theta + g\,w\,s_\theta \end{pmatrix}$$

$$\mathbf{J_q} = \begin{pmatrix} j_{q11} & 0 & 0 & 0 \\ 0 & j_{q22} & 0 & 0 \\ 0 & 0 & j_{q33} & 0 \\ 0 & 0 & 0 & j_{q44} \end{pmatrix}$$

with $\begin{cases} j_{q11} = b\,r\,c_1 - a\,r\,s_1\,; \ \ j_{q22} = f\,r\,c_2 - e\,r\,s_2 \\ j_{q33} = d\,r\,c_3 - c\,r\,s_3\,; \ \ j_{q44} = h\,r\,c_4 - g\,r\,s_4 \end{cases}$

The direct differential model can be obtained through the Jacobian matrix $\mathbf{J} = \mathbf{J_x}^{-1}\mathbf{J_q}$ when $\mathbf{J_x}$ is invertible.

If $\mathbf{J_x}$ or $\mathbf{J_q}$ is not a full rank matrix it means that the robot is in a singular configuration.
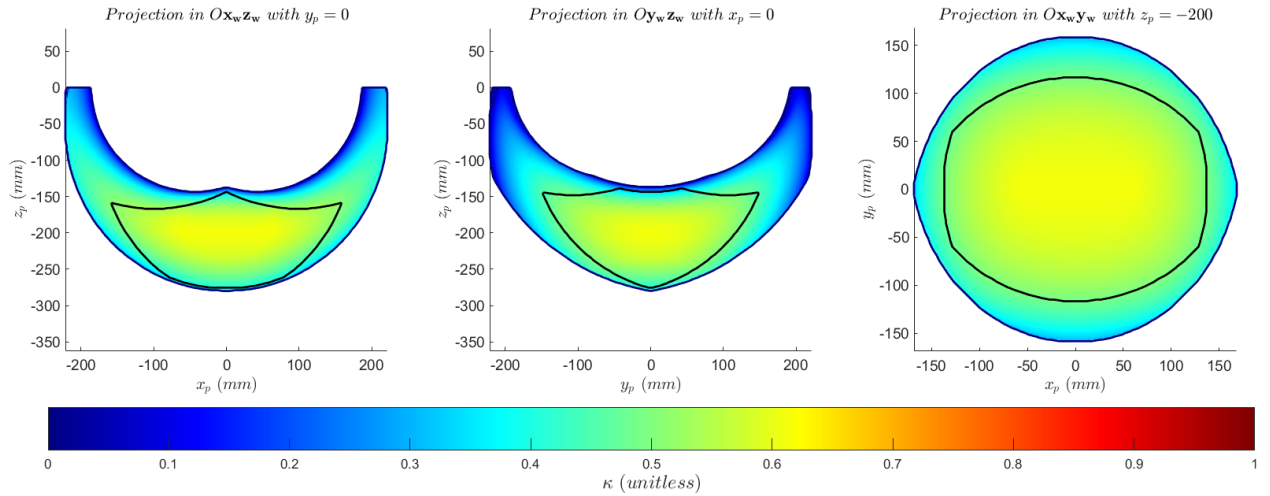
Figure 5. Sectional views of the workspace with the value of the inverse condition number κ as a colormap for an angle of the platform $\theta = -\frac{\pi}{4}$. The figure gives the boundary of the workspace without limitations (in blue) and with actuator strokes (in black). The robot will be used in the red part of the workspace.

V. Workspace analysis

A. Translational workspace

The translational workspace of the manipulator has been computed numerically for different angles θ of the platform using a discretized cartesian space of $\mathbf{x} = (x_p; y_p; z_p; \theta)$. The workspace is calculated as the collection of the discrete poses respecting the condition (7) established from the inverse model. The boundaries of the workspace have been determined numerically, with the dimension of the experimental manipulator given in section VI-A, and are drawn in blue in the sectional views in the Fig. 5.

Moreover, a second workspace named "reduced workspace" taking into account the experimental constraints has also been calculated. This reduced workspace, whose boundaries are drawn in black on Fig 5, contains also the poses respecting the actuators strokes between 45° and -85°.

B. Numerical computation of the manipulability

For a given constant angle θ, the manipulator has all Delta robot singularities. In addition, it has specific singularities due to the folding motion of its platform. In particular, the configuration is singular if the forearms A_2B_2 or A_4B_4 are respectively coplanar with the left and right parts of the platform.

To compute the singular configurations, we considered two complementary cases decomposing both types of movements: platform translations and its folding. The first case considers the translation motion capability when the angle θ of the platform remains constant while the second one considers the capability to fold the platform at a given position.

C. Translational manipulability

To draw the manipulability index of the robot with a constant θ angle, the inverse condition number κ has been considered [30]–[32]:

$$\kappa = \sqrt{\frac{\lambda_{min}(\mathbf{GG^T})}{\lambda_{max}(\mathbf{GG^T})}} \qquad (9)$$

where $\mathbf{G}$ is the submatrix composed of the 3 first lines of the Jacobian $\mathbf{J}$, $\lambda_{max}(\cdot)$ and $\lambda_{min}(\cdot)$ are the functions providing respectively the maximum and minimum eigen values of a matrix. The closer to 1 κ is, the better is the control of the robot. A low value indicates a poor manipulability and 0 a singular configuration. The enclosed video presents the evolution of the workspace and the value of κ for platform angle θ from $-\frac{\pi}{2}$ to $\frac{\pi}{2}$. The video shows that for positive angle θ there are central areas in which κ is close to zero. Notably, some singular configurations appear in the reduced workspace for θ values around $\frac{\pi}{4}$. On the contrary, when the angle is negative, the reduced workspace has a relatively high κ index which indicates a good manipulability of the robot. For instance, when $\theta = -\frac{\pi}{4}$ (see Fig. 5) κ is over 0.5 in the majority of the surface and always greater than 0.3.

D. Rotational manipulability

The second part of the analysis concerns the capability to fold the platform to an angle θ in order to actuate the gripper at a given position of the workspace (x_p, y_p, z_p). As the platform has only one degree of freedom, the κ index cannot be applied and the following manipulability index has been considered:

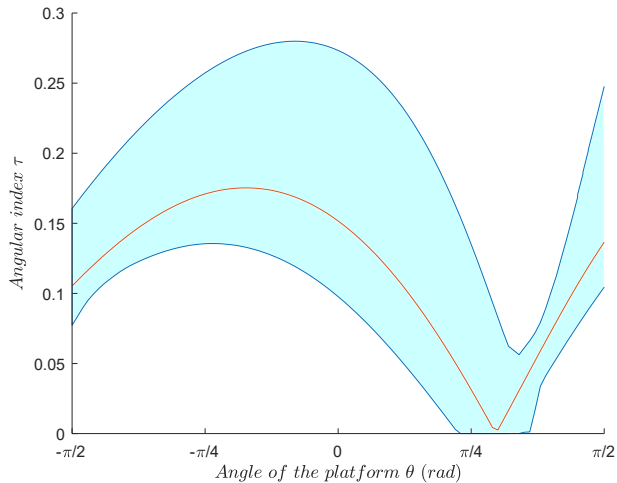$$\tau = \sqrt{\frac{1}{\mathbf{HH^T}}} \qquad (10)$$

Figure 6. Platform manipulability index τ versus the angle of the platform θ over the reduced workspace. The hull is determined by a discretization of the reduced workspace which leads to 51 624 positions. The red line represents the evolution of τ for the position $x_p = 0$, $y_p = 0$ and $z_p = -200$.

Figure 7. Experimental prototype of the proposed robotic structure and zoom in on the gripper.

where **H** is the last line of the Jacobian matrix **J**. Contrary to κ, τ is not normalized. But like κ, when τ reaches a zero value, it indicates a singular configuration where the transmission ratio between the joints and θ is infinity. Conversely, a large value means a very low transmission ratio.

The evolution of τ within the sectional views of the workspace is described in the enclosed video. We focused the study on the reduced workspace in which 51 624 different positions (x_p, y_p, z_p) have been considered in order to evaluate the capability to actuate the folding of the platform. Those positions are obtain by a discretization of the workspace along the three translation with a constant step. For each position, 101 values of θ uniformly distributed in $[-\frac{\pi}{2}; \frac{\pi}{2}]$ have been taken. It provides a series of 51 624 curves showing the evolution of τ in function of θ (e.g. red curve in Fig. 6). The hull of this series of curves has been also computed and is represented in cyan on Fig. 6. It shows that for an angle of the platform near $\frac{\pi}{4}$, it exists at least one position within the workspace in which it is not possible to control the folding of the platform as the angular index τ is equal to zero. Moreover, it shows that the most convenient angles for the platform is around $-\frac{\pi}{4}$ where the index τ stays over 0.1. It allows to actuate θ in both directions with good transmission ratio everywhere in the reduced workspace.

Consequently, the home position has been designed in order to have a platform angle $\theta = -\frac{\pi}{4}$.

VI. Experimental validation
A. Prototype design

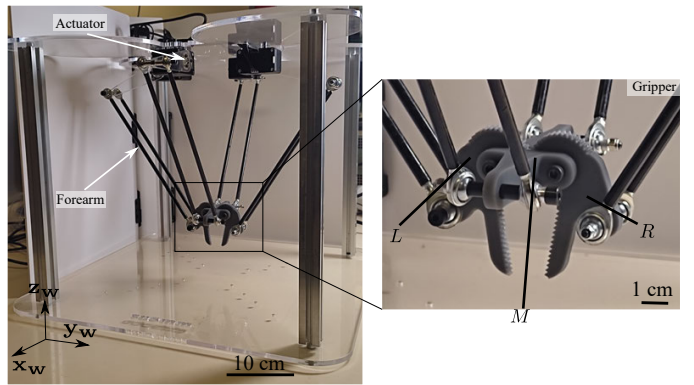To validate the proposed robotic structure a proof-of-principle prototype has been designed and realized using

four Dynamixel XM430-W210-R servomotors, steel ball joints, carbon tubes, and 3D printed parts. The gearwheel is composed of 40 teeth considering its whole revolution (see Fig. 7).

The design parameters of this prototype have been selected with proportions similar to the Ix4 Omron robot that are given by the following guidelines:

$$r \approx 2(k-u) \approx \frac{l}{3}$$

The final lengths of the prototype are $k = 82.5$mm, $r = 80$mm, $l = 223$mm, $u = 40$mm, $v = 13.5$mm, and $w = 26.5$mm.

B. Experimental results

Experimental validation of different displacements have been achieved using the inverse kinematic model. The manipulator is able to follow trajectories for both joint-space point-to-point motions and Cartesian interpolated motions. The displacements were made with the maximum speed (70 rpm) of the Dynamixel actuators and can be much appreciated in the accompanying video.

The first displacements made are those along the three directions $\mathbf{x_w}$, $\mathbf{y_w}$ and $\mathbf{z_w}$. This first experiment shows that the angle of the platform does not change during this type of displacements which is important for the manipulation of objects.

With the designed prototype the angle of the platform can be adjusted from $-\frac{\pi}{3}$ to $-\frac{\pi}{6}$, which gives the opportunity to open and close the gripper and to keep index τ over 0.1. Moreover, given the speed of the actuators, the change of the angle of the platform from $\theta = -\frac{\pi}{4}$ to $\theta = -\frac{\pi}{3}$ leading to the closing of the gripper is performed within 60 ms.

To illustrate the pick-and-toss capability, several objects have been tested. First a wine cork, which is a cylinder with a diameter of 24 mm and a height of 45 mm, has been manipulated as shown in Fig. 8. The robot starts by moving along the $\mathbf{z_w}$ axis. Then, the cork is picked up and moved to another position using joint-space point-to-point
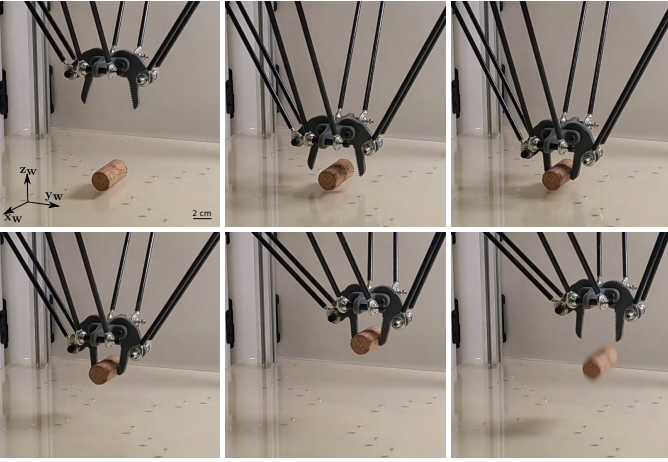
Figure 8. Pick-and-toss of a cork using displacement along $\mathbf{z_w}$-axis (50 mm) and $\mathbf{y_w}$-axis (70 mm).

motions along the $\mathbf{z_w}$ and $\mathbf{y_w}$ axes. Finally, the object is dropped by opening the gripper. The displacements achieved is around 50 mm along $\mathbf{z_w}$ and 70 mm along $\mathbf{y_w}$. During this cycle, the angle of the platform and consequently the closing of the gripper remains constant ensuring than the cork is not released during the displacement.

Then others pick-and-toss cycles have been also performed by collecting a bottle cap and a parallelepiped rubber into a tray. For these tests, the displacements are joint-space point-to-point motions done at full speed with synchronized trapezoidal velocity profiles. This experiments give the opportunity to show that the angle of the platform remains constant whatever the θ value ensuring that objects with different sizes and shapes can be carried from the pick position to the toss position.

Other experiments have been conducted. Notably, a circular trajectory using a Cartesian interpolated motion has been executed, with a radius of 80 mm which covers almost 80% of the reduced workspace, in the $(O, \mathbf{x_w}, \mathbf{y_w})$ plane with the gripper in opened and closed positions showing also that the angle θ remains unchanged during interpolated trajectories.

All the described experiments can be seen in the accompanying video.

VII. Discussion

The developed robotic architecture paves the way to new solutions with integrated grasping in the context of waste sorting. The presented prototype is a first proof-of-concept. Some additional works will be done in the future in order to improve the speed of motion and to control the grasping force. The current results illustrate the capability of the structure to actuate an embedded gripper while generating the three translations.

Depending on the class of objects to pick, the design of the gripper can be adapted. For heavy materials, scissor lifters or lifting clamps are probably more suitable. These inverted gripper can be used to take benefit from the weight of the grasped object to maintain the gripper closed. If needed, parallel jaw grippers with circular translation can also be mounted on the platform.

The most important improvement related to the grasping is the control of clamping force. Indeed, when manipulating a rigid object the mechanism becomes hyperstatic. To avoid a possible loss of objects during transportation, it is required to introduce some compliance in the structure. This can be done by passive or active ways. For instance, the gripper jaws could be fabricated with a soft material. Another solution would be to introduce of a rotation spring between the platform parts and the fingers. Active compliance control could be implemented as well. This architecture is particularly well adapted for position-force control since it includes a minimal number of mechanical parts between the actuators and the fingers. Moreover, the transmission ratios, computed as the inverse of τ, is between 3.4 and 10.3 in the reduced workspace.

Finally, the increase of the robot speed could be done by integrating industrial actuators and by redesigning the mechanical parts to reduce the inertia at most while maintaining a sufficient endurance.

VIII. Conclusion

In this paper, a new robotic architecture has been proposed and developed. A first experimental setup has been realized to validate the concept of this robot which can achieve pick-and-toss applications thanks to the three translations and the gripping capability. The main originality is that the gripper is fully integrated into the 4-DoF parallel robotic structure. There are several advantages to this solution as less inertia and mass are embedded on the robot's platform compared to classical solutions. Moreover, the power of the actuators is used to close and open the gripper so there is no need for additional electrical or pneumatic connections to actuate the gripper. As the actuation of the gripping part is deported onto the base of the robot, it is distant from the dusty and wet environment which should improve the lifetime of the proposed system for waste sorting applications. For picking object with various orientations, several manipulators with different orientation can be placed on the sorting line to cover all the encountered cases.

References

[1] B. Taylor, "How robots are revolutionizing recycling," *Recycling today*, January 30 2019. [Online]. Available: https://www.recyclingtoday.com/article/recycling-robots-ai-sorting/

[2] H. Wilts, B. R. Garcia, R. G. Garlito, L. S. Gómez, and E. G. Prieto, "Artificial intelligence in the sorting of municipal waste as an enabler of the circular economy," *Resources*, vol. 10, no. 4, p. 28, 2021.

[3] S. P. Gundupalli, S. Hait, and A. Thakur, "A review on automated sorting of source-separated municipal solid waste for recycling," *Waste management*, vol. 60, pp. 56–74, 2017.

[4] K. Pyzyk, "Robots move in," *Waste dive*, December 11 2019. [Online]. Available: https://www.wastedive.com/news/recycling-labor-mrf-robots-move-in/568554/

[5] J.-P. Merlet, *Parallel robots.* Springer Science & Business Media, 2006.

[6] R. Clavel, "A fast robot with parallel geometry," in *Proceedings of the International Symposium on Industrial Robots*, 1988, pp. 91–100.

[7] F. Pierrot, C. Reynaud, and A. Fournier, "Delta: a simple and efficient parallel robot," *Robotica*, vol. 8, no. 2, pp. 105–109, 1990.

[8] J. Pransky, "The pransky interview: Dr. matanya horowitz, founder and CEO of AMP robotics," *Industrial Robot*, vol. 47, no. 3, pp. 319–323, 2020.

[9] T. J. Lukka, T. Tossavainen, J. V. Kujala, and T. Raiko, "Zenrobotics recycler–robotic sorting using machine learning," in *Proceedings of the International Conference on Sensor-Based Sorting (SBS)*, 2014, pp. 1–8.

[10] Y.-D. Ku, J.-H. Yang, H.-Y. Fang, W. Xiao, and J.-T. Zhuang, "Optimization of grasping efficiency of a robot used for sorting construction and demolition waste," *International Journal of Automation and Computing*, vol. 17, no. 5, pp. 691–700, 2020.

[11] F. Raptopoulos, M. Koskinopoulou, and M. Maniadakis, "Robotic pick-and-toss facilitates urban waste sorting," in *Proceedinds of the IEEE International Conference on Automation Science and Engineering (CASE)*, 2020, pp. 1149–1154.

[12] F. Pierrot, F. Marquet, O. Company, and T. Gil, "H4 parallel robot: modeling, design and preliminary experiments," in *Proceedings of the IEEE International Conference on Robotics and Automation (ICRA)*, vol. 4, 2001, pp. 3256–3261.

[13] V. Nabat, M. de la O Rodriguez, O. Company, S. Krut, and F. Pierrot, "Par4: very high speed parallel robot for pick-and-place," in *Proceedings of the IEEE/RSJ International conference on intelligent robots and systems (IROS)*, 2005, pp. 553–558.

[14] J. Angeles, S. Caro, W. Khan, and A. Morozov, "Kinetostatic design of an innovative schönflies-motion generator," *Journal of Mechanical Engineering Science*, vol. 220, no. 7, pp. 935–943, 2006.

[15] G. Wu, S. Bai, and P. Hjørnet, "Architecture optimization of a parallel schönflies-motion robot for pick-and-place applications in a predefined workspace," *Mechanism and Machine Theory*, vol. 106, pp. 148–165, 2016.

[16] L.-T. Schreiber and C. Gosselin, "Schönflies motion parallel robot (spara): a kinematically redundant parallel robot with unlimited rotation capabilities," *IEEE/ASME Transactions on Mechatronics*, vol. 24, no. 5, pp. 2273–2281, 2019.

[17] Penta Robotics, "Veloce robot." [Online]. Available: http://pentarobotics.com/products/

[18] B.-J. Yi, H. Y. Na, J. H. Lee, Y.-S. Hong, S.-R. Oh, I. H. Suh, and W. K. Kim, "Design of a parallel-type gripper mechanism," *The International Journal of Robotics Research*, vol. 21, no. 7, pp. 661–676, 2002.

[19] S. Hamaza, P. Lambert, M. Carricato, and J. Herder, "The quadrog robot, a parallel robot with a configurable platform for haptic applications," in *Proceedings of the ASME International Design Engineering Technical Conferences and Computers and Information in Engineering Conference*, vol. 57144, 2015.

[20] P. Lambert and J. Herder, "A novel parallel haptic device with 7 degrees of freedom," in *Proceedings of the IEEE World Haptics Conference (WHC)*, 2015, pp. 183–188.

[21] K. Wen, D. Harton, T. Laliberté, and C. Gosselin, "Kinematically redundant (6+ 3)-dof hybrid parallel robot with large orientational workspace and remotely operated gripper," in *Proceedings of the IEEE International Conference on Robotics and Automation (ICRA)*, 2019, pp. 1672–1678.

[22] C. Gosselin, T. Laliberté, and A. Veillette, "Singularity-free kinematically redundant planar parallel mechanisms with unlimited rotational capability," *IEEE Transactions on Robotics*, vol. 31, no. 2, pp. 457–467, 2015.

[23] M. Isaksson, C. Gosselin, and K. Marlow, "An introduction to utilising the redundancy of a kinematically redundant parallel manipulator to operate a gripper," *Mechanism and Machine Theory*, vol. 101, pp. 50–59, 2016.

[24] W. Haouas, R. Dahmouche, N. Le Fort-Piat, and G. J. Laurent, "A new seven degrees-of-freedom parallel robot with a foldable platform," *Journal of Mechanisms and Robotics*, vol. 10, no. 4, p. 045001, 2018.

[25] ——, "4-DoF spherical parallel wrist with embedded grasping capability for minimally invasive surgery," in *Proceedings of the IEEE/RSJ International Conference on Intelligent Robots and Systems (IROS)*, Oct. 2016, pp. 2363–2368.

[26] W. Haouas, G. J. Laurent, S. Thibaud, and R. Dahmouche, "Kinematics, design and experimental validation of a novel parallel robot for two-fingered dexterous manipulation," in *Proceedings of the IEEE/RSJ Interntational Conference on Intelligent Robots and Systems (IROS)*, 2019, pp. 6763–6768.

[27] R. Dahmouche, K. Wen, and C. Gosselin, "Transferability in an 8-dof parallel robot with a configurable platform," in *Proceedings of the IEEE/RSJ International Conference on Intelligent Robots and Systems (IROS)*, 2020, pp. 6544–6549.

[28] J. Lenarčič and B. Siciliano, *Advances in Robot Kinematics 2020.* Springer Nature, 2020, vol. 15.

[29] W. Khalil and E. Dombre, *Modeling identification and control of robots.* CRC Press, 2002.

[30] J.-P. Merlet, "Jacobian, manipulability, condition number, and accuracy of parallel robots," *ASME J. of Mechanical Design*, vol. 128, pp. 199–206, 2006.

[31] S. Botello-Aceves, S. I. Valdez, H. M. Becerra, and E. Hernandez, "Evaluating concurrent design approaches for a delta parallel manipulator," *Robotica*, vol. 36, no. 5, p. 697–714, 2018.

[32] S. Patel and T. Sobh, "Manipulator performance measures-a comprehensive literature survey," *Journal of Intelligent & Robotic Systems*, vol. 77, no. 3, pp. 547–570, 2015.